Symposium

Unveiling the Extracellular Space of the Brain: From Super-resolved Microstructure to *In Vivo* Function

Sabina Hrabetova,[1] Laurent Cognet,[2,3] Dmitri A. Rusakov,[4] and U. Valentin Nägerl[5,6]

[1]Department of Cell Biology, State University of New York Downstate Medical Center, Brooklyn, New York 11203, [2]Université de Bordeaux, Laboratoire Photonique Numérique et Nanosciences, F-33400 Talence, France, [3]Institut d'Optique and Centre National de la Recherche Scientifique, F-33400 Talence, France, [4]Institute of Neurology, University College London, London WC1N 3BG, United Kingdom, [5]Institut Interdisciplinaire des Neurosciences, Université de Bordeaux, 33077 Bordeaux, France, and [6]Institut Interdisciplinaire des Neurosciences, Centre National de la Recherche, 33077 Bordeaux, France

The extracellular space occupies approximately one-fifth of brain volume, molding a spider web of gaps filled with interstitial fluid and extracellular matrix where neurons and glial cells perform in concert. Yet, very little is known about the spatial organization and dynamics of the extracellular space, let alone its influence on brain function, owing to a lack of appropriate techniques (and a traditional bias toward the inside of cells, not the spaces in between). At the same time, it is clear that understanding fundamental brain functions, such as synaptic transmission, memory, sleep, and recovery from disease, calls for more focused research on the extracellular space of the brain. This review article highlights several key research areas, covering recent methodological and conceptual progress that illuminates this understudied, yet critically important, brain compartment, providing insights into the opportunities and challenges of this nascent field.

Key words: **extracellular space; extracellular matrix; diffusion; super-resolution microscopy; carbon nanotubes; SUSHI**

Introduction

Each brain cell is separated from its neighbors by a narrow gap, the extracellular space (ECS) (Fig. 1*A*), which contains interstitial fluid, the extracellular matrix, and other secreted molecules. All gaps are interconnected and form a complex 3D structure that occupies ~20% of the brain (Nicholson and Hrabetová, 2017), and this value is largely conserved from octopus to human (Syková and Nicholson, 2008). The ECS is not a static compartment, but it changes during physiological brain activity and sleep as well as over the course of brain disorders (Syková and Nicholson, 2008; Xie et al., 2013; Nicholson and Hrabetová, 2017). Although the ECS has traditionally received much less attention than neuronal and glial networks, it plays a fundamental functional role in brain health and disease. The ECS serves as a reservoir of ions for electrical activity, and it provides an essential microenvironment for the well-being of cells and brain homeostasis. The ECS spawns the physical corridor for diffusion-mediated transport of substances; over relatively short distances (tens to hundreds of nanometers), as in the case of chemical synapses and extrasynaptic receptors, as well as for much longer distances (micrometers to centimeters), as in the case of volume transmission and metabolite removal, where bulk flow may come into play. Ineffective removal of proteins released into the ECS, such as α-synuclein, amyloid-β, and tau, may contribute to the progression of neurodegenerative diseases (Iliff et al., 2014). The ECS also forms the final route for transport of therapeutic agents entering the brain through the blood–brain barrier or by direct injection, and thus is of high clinical importance.

We will summarize results from biophysical experiments and numerical modeling, which single out the factors that influence molecular diffusion in the ECS, such as anatomical geometry, interstitial viscosity, charge interactions, steric hindrance, and physical drag. We will then review recent evidence for extracellular micro-viscosity, which shapes the profile of synaptic receptor activation by released neurotransmitter molecules. Finally, we will present two recent optical approaches based on super-resolution microscopy (single-molecule imaging of carbon nanotubes [CNT] and super-resolution shadow imaging [SUSHI]) that can visualize the (dynamic) nanoscale spatial topology of the ECS and extract information about its local viscosity and volume fraction in living brain tissue.

Exploring the structure and function of brain ECS with biophysical and computational methods

Established approaches to study the structure of brain ECS use diffusion of molecular probes, such as radiotracers, ions, or fluorescently labeled macromolecules (Nicholson and Hrabetová, 2017). In a diffusion experiment, these probes are injected at a defined location into the ECS from where they are monitored in time as they explore the ECS (Fig. 1*B*). Biophysical analysis of the diffusion data quantifies two major structural parameters of the ECS: diffusion permeability and volume fraction. The diffusion

Received July 29, 2018; revised Sept. 25, 2018; accepted Sept. 26, 2018.

S.H. thanks Charles Nicholson for developing Real-Time Iontophoresis and Integrative Optical Imaging methods. L.C. thanks Erwan Bézard and Laurent Groc for helpful discussions. D.A.R. thanks K. Zhen and K. Suhling for driving the development of time-resolved fluorescence anisotropy imaging. U.V.N. thanks the SUSHI chefs Jan Tønnesen and Krishna Inavalli.

The authors declare no competing financial interests.

Correspondence should be addressed to Dr. U. Valentin Nägerl, Institut Interdisciplinaire des Neurosciences, Université de Bordeaux, 146 Rue Leo Saignat, Bordeaux 33077, France. E-mail: valentin.nagerl@u-bordeaux.fr.

DOI:10.1523/JNEUROSCI.1664-18.2018

 0270-6474/18/389355-09$15.00/0

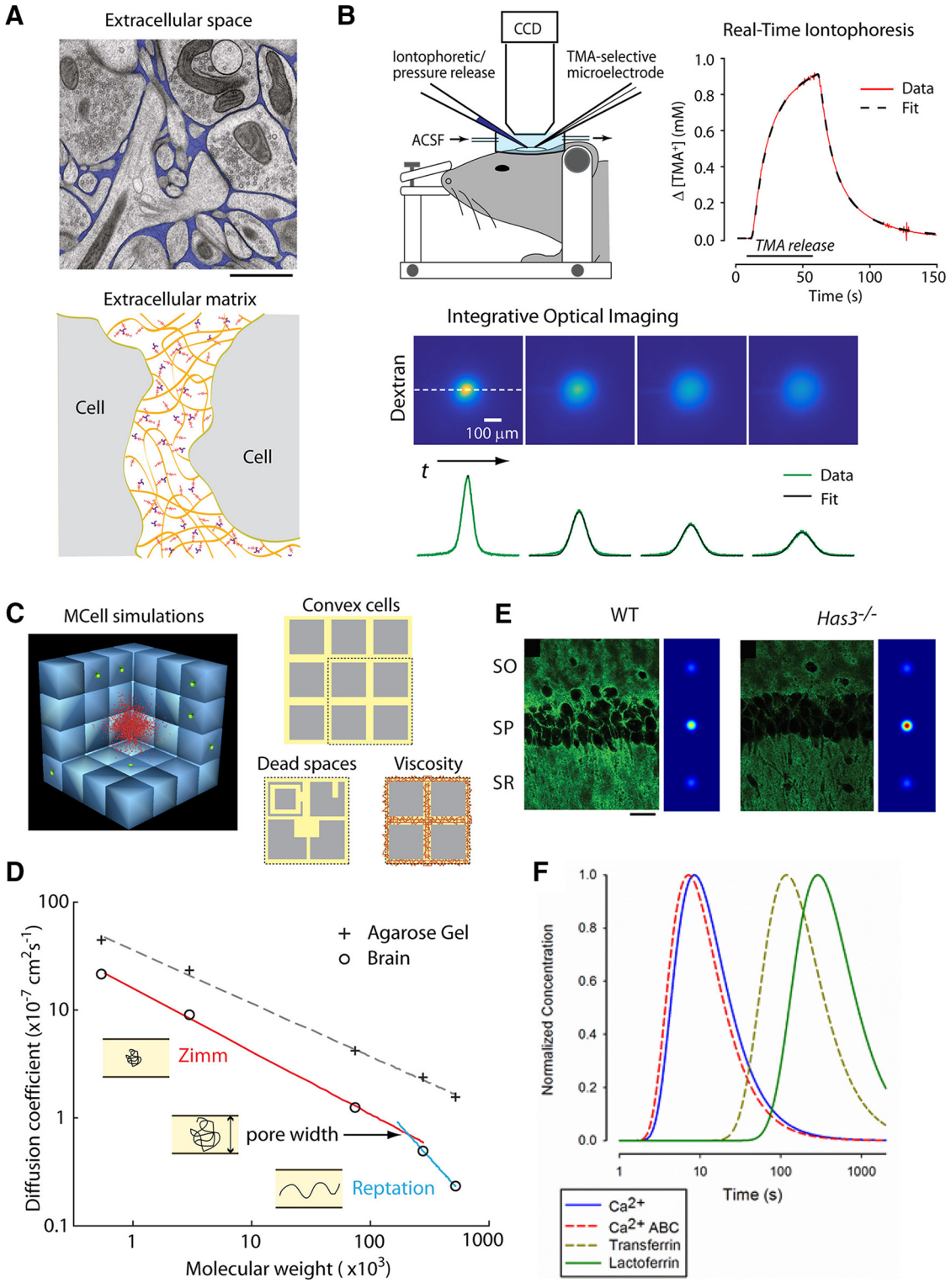

Figure 1. Structure of brain ECS studied with diffusion experiments and numerical simulations. ***A***, Top, ECS colored in blue in the electron micrograph of mouse cerebral cortex processed with cryofixation. Scale bar,1 μm. Photograph courtesy of Korogod et al. (2015). Bottom, Schematic of extracellular matrix residing in the ECS. Image courtesy of Odackal et al. (2017). ***B***, Two diffusion-based methods, real-time iontophoresis (Nicholson and Phillips, 1981), and integrative optical imaging (Nicholson and Tao, 1993), quantify ECS parameters in brain slices and *in vivo*. In real-time iontophoresis, a small ion (typically the cation tetramethyammonium [TMA], 74 MW), is iontophoretically released and detected by an ion-selective microelectrode positioned ~100 μm away; θ and α are quantified. In integrative optical imaging, fluorophore-labeled macromolecules are released by pressure injection and the diffusing cloud is detected with a CCD camera; θ is quantified. ***C***, Left, Example of a 3D model used for numerical simulations of extracellular diffusion with MCell; cells in the middle were removed to show diffusing particles (red dots). Image reproduced with permission from Xiao et al. (2015). Right, Three models: ECS surrounding convex cells, ECS containing dead-space microdomains, viscous ECS. ***D***, Scaling theory obtains the average ECS width from the diameter of a flexible dextran polymer compelled to switch from a coiled shape diffusing in a Zimm regimen to an uncoiled shape diffusing in a reptation regimen. Plot reproduced with permission from Xiao et al. (2008). ***E***, Hyaluronan, stained with hyaluronic acid binding protein (green), is reduced in the CA1 region of hippocampus of hyaluronan synthase 3 knocked out (*Has3* $^{-/-}$) mice. Simulation of diffusion shows that the concentration of released molecules (at 10 ms time point) is the highest in the stratum pyramidale of *Has3* $^{-/-}$ mice where the ECS volume is only 7% (vs 12% in wild type). WT, wild type; SO, stratum oriens; SP, stratum pyramidale; SR, stratum radiatum. Scale bar, 30 μm. Images courtesy of Arranz et al. (2014). (*Figure legend continues.*)

permeability (θ) represents the hindrance that slows down the diffusing molecules in tissue compared with an obstacle-free medium ($\theta = D^*/D$; D^* is the effective diffusion coefficient, D is the free diffusion coefficient), which is also reported as tortuosity ($\lambda = (1/\theta)^{0.5}$), and the volume fraction (α) denotes the percentage of a given brain area that is occupied by the ECS ($\alpha = V_{ECS}/V_{tissue}$). Averaged over the gray matter of the brain, θ is ~0.39 for small molecules and α ~0.2 (meaning, ~20% of the brain is ECS) (Nicholson and Hrabetová, 2017). Diffusion permeability decreases with hydrodynamic diameter of the molecule, and it was reported to be as low as 0.0089 for quantum dots (QDs) with a hydrodynamic diameter of 35 nm (Nicholson and Tao, 1993; Thorne and Nicholson, 2006). These values of θ and α were measured under physiological conditions in adult brain tissue, but they depend greatly on brain region, developmental stage, and pathological conditions (Syková and Nicholson, 2008).

The interpretation of θ has often been difficult because it was not clear which structural elements of the complex ECS environment impede the diffusing molecules. This long-standing question was addressed by combining measurements in brain tissue with theoretical work and Monte Carlo diffusion simulations (Stiles and Bartol, 2001) (Fig. 1*C*). It was thought that the hindrance can be explained by mere circumnavigation of diffusing molecules around convex cells. However, θ derived theoretically or obtained from simulations in media composed of convex cells explained only approximately one-third of hindrance measured in brain ECS (Hrabetová et al., 2003; Hrabe et al., 2004; Tao and Nicholson, 2004). It was hypothesized that the remaining hindrance could arise from dead-space microdomains that transiently delay diffusing molecules or from extracellular viscosity (Rusakov and Kullmann, 1998; Hrabetová and Nicholson, 2004) (Fig. 1*C*). The inclusion of dead-space microdomains (spaces surrounded by concave astrocytic wrappings, spaces inside cell invaginations, or voids between cells) increases the hindrance in computational models to experimental values obtained in brain ECS (Hrabe et al., 2004; Tao et al., 2005). Recent studies of nanoscale diffusion in the interstitial gaps using time-resolved fluorescence anisotropic imaging found that viscosity accounted for approximately one-third of hindrance measured in brain ECS (Zheng et al., 2017). Together, these results indicate that convex cells, dead spaces, and viscosity each contribute approximately one-third to the diffusional hindrance of brain ECS. Application of dwell-time diffusion theory (Hrabe et al., 2004) to these data indicates that approximately one-fourth of the ECS volume resides in dead-space microdomains.

Importantly, extracellular hindrance depends greatly on molecular size, being much higher for larger substances, such as endogenous proteins, liposomal and viral drug carriers, therapeutics than for small molecules, such as neurotransmitters or ions (Nicholson and Tao, 1993; Thorne and Nicholson, 2006; Xiao et al., 2008). Application of the scaling theory of polymer diffusion (de Gennes, 1979) or the theory of restricted diffusion in pores (Deen, 1987; Dechadilok and Deen, 2006) to ECS diffusion offers the opportunity to estimate the width of gaps between the cells where macromolecules diffuse. Applying scaling theory to diffusion of flexible polymers in an isolated turtle cerebellum, ECS width was estimated to be 31 nm (Xiao et al., 2008) (Fig. 1*D*), whereas applying restricted diffusion theory to the diffusion of dextrans and QDs in rat neocortex *in vivo* led to estimates of 38 or 64 nm depending on whether the ECS was assumed to be composed of sheets or interconnected cylinders (Thorne and Nicholson, 2006). These studies indicate that the gaps between the cells are at least 2–4 times wider than estimates based on electron microscopy (EM) using chemical fixation.

The ECS contains the extracellular matrix, which is composed of a mesh of glycosaminoglycans, proteoglycans, and small proteins (Fig. 1*A*). A major component of the extracellular matrix is the large polysaccharide hyaluronan, an anionic glycosaminoglycan. Hyaluronan's high levels of hydration, together with its rapid synthesis directly into the ECS (Toole, 2004), could constitute a mechanism that maintains and regulates ECS volume. Removal of the gene for hyaluronan synthase 3 leads to hyaluronan deficiency in hippocampal CA1 region, a 40% reduction of ECS volume in stratum pyramidale (Fig. 1*E*) and an epileptic phenotype (Arranz et al., 2014), in line with the epileptiform activity induced by enzymatic digestion of hyaluronan *in vitro* (Vedunova et al., 2013). Reduced ECS volume might promote epileptiform activity via a variety of mechanisms, including (1) elevated concentrations in the ECS of neuroactive molecules or ions (e.g., K^+ and Ca^{2+}), which would tend to promote synaptic transmission, neuronal excitability, and firing in nearby neurons; and (2) increased excitatory ephaptic interactions due to closer apposition of neuronal membranes (Jefferys, 1995). In any case, hyaluronan plays a pivotal for the maintenance of ECS volume and normal brain activity (Perkins et al., 2017). Other components of the extracellular matrix include negatively charged proteoglycans, especially heparan sulfate and chondroitin sulfate, and a group of small proteins that interconnect matrix macromolecules and stabilize its structure. Because proteoglycans are negatively charged, they electrostatically interact with positively charged substances diffusing in the ECS. Indeed, heparan sulfate proteoglycan and the positively charged lactoferrin protein bind to each other in a fast, reversible, and charge-dependent way (Thorne et al., 2008) (Fig. 1*F*), and charge-based interactions between calcium and chondroitin sulfate proteoglycan were reported, where enzymatic removal of negatively charged chondroitin sulfate groups increased diffusion permeability for calcium (Fig. 1*F*), but not for monovalent cation tetramethylammonium (Hrabetová et al., 2009). ECS volume was preserved in brain tissue treated with chondroitinase ABC, indicating that chondroitin sulfate proteoglycans are not involved in ECS volume maintenance, unlike hydrated hyaluronan. Despite these and other recent advances (Ferrer-Ferrer and Dityatev, 2018), the extracellular matrix remains a poorly understood compartment in the mammalian brain.

ECS viscosity shapes the fate of released neurotransmitters

Rapid diffusion of signaling molecules inside nanoscopic gaps between cells is a basic process underpinning activity of brain circuits. The way neurotransmitter molecules diffuse in the interstitial space determines where and to what degree their target receptors are activated, inside and outside the synaptic cleft. This issue has gained much attention in the context of common excitatory synapses operating ionotropic AMPA-type glutamate receptors, which are critical to rapid information transfer across neural circuits of the brain. AMPA receptors feature relatively low affinity to their ligand, the excitatory neurotransmitter glutamate; therefore, their activation depends strongly on the mag-

←

(*Figure legend continued.*) ***F***, Simulated diffusion curves (at 100 μm away from the source) show that calcium diffusion is enhanced after enzymatic removal of negatively charged components of the extracellular matrix with chondroitinase ABC and that protein lactoferrin with positively charged binding sites for the extracellular matrix diffuses more slowly than protein transferrin that is similar in size but lacks the binding sites. Plot reproduced with permission from Nicholson and Hrabetová (2017).

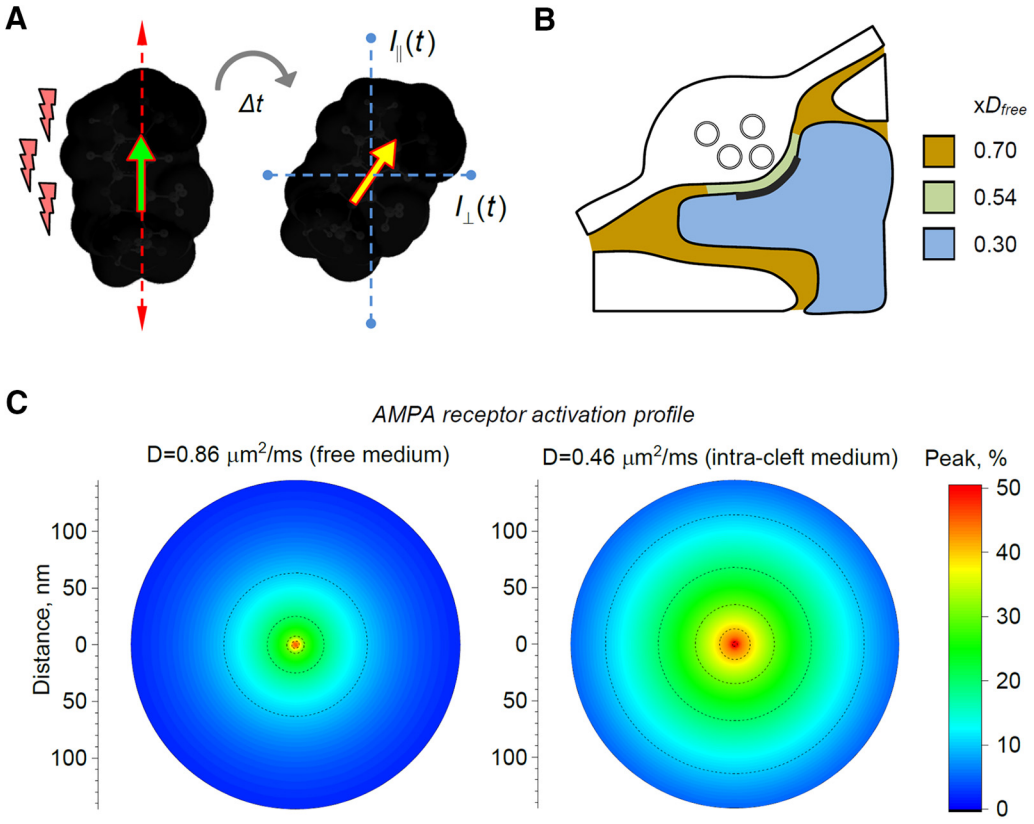

Figure 2. Molecular diffusivity on the nanoscale shapes the activation profile of AMPA receptors in the cleft. ***A***, Diagram illustrating the principle of measuring nano-viscosity (quasi-instantaneous diffusion) using time-resolved fluorescence anisotropy imaging (TR-FAIM). A fluorescent probe molecule (dark shape) excited with a femtosecond pulse of polarized light (left; red lightings indicate light pulse; arrows indicate light polarization plane; yellow arrow indicates molecular excitation plane) moves and gyrates in space before emitting a photon at $t = \Delta t$ at a new angle (yellow arrow). The emission intensity is recorded through two perpendicular analyzers (blue dotted lines, $I_{\rho}(t)$ and $I_{\wedge}(t)$): because molecular gyration directly depends on local micro-viscosity the analytical relationship between the two signals can be translated into instantaneous diffusivity (Zheng et al., 2014; Suhling et al., 2015). ***B***, Diagram illustrating experimental measurements of nano-viscosity in acute hippocampal slices (area CA3) using TR-FAIM (Zheng et al., 2017). Colors and labels (xD_{free}) indicate average diffusion retardation factors compared with free-medium diffusion in ACSF. ***C***, Simulated profiles of AMPAR receptor activation (peak percentage of open receptors, color scale) upon release of 2800 glutamate molecules into the synaptic cleft at two glutamate diffusion coefficients: one in a free-medium ACSF (0.86 μm^2/ms) and one between presynaptic and postsynaptic membranes (0.46 μm^2/ms) measured using TR-FAIM (Zheng et al., 2017), as indicated. The data reflect Monte Carlo simulations replicating the function of common excitatory synapses (modeled on hippocampal CA3-CA1 connections) (Savtchenko et al., 2013; Savtchenko and Rusakov, 2014; Zheng and Rusakov, 2015).

nitude and spatial extent of local glutamate transients. Because it has not been possible to resolve or detect such events with existing experimental tools, quantitative insights have come from biophysical models incorporating synaptic architecture and its environment (Clements, 1996; Wahl et al., 1996; Trommershäuser et al., 1999; Rusakov, 2001). More recent incarnations of such modeling have involved Monte Carlo simulations, which trace the fate of individual glutamate molecule and their interactions with individual receptors, inside and outside the cleft.

Computer simulations have predicted that, given the same amount of released glutamate, AMPA receptor activation could depend strongly on the distance between the release site and receptor for glutamate (Raghavachari and Lisman, 2004; Zheng et al., 2008; Kinney et al., 2013; Savtchenko et al., 2013). It has been proposed that only a small, perhaps 100–150 nm wide, local cluster of AMPA receptors will be activated upon synaptic discharges (Rusakov, 2001; Raghavachari and Lisman, 2004). This concept took on additional significance when (super-resolution) single-particle tracking studies began to show prominent receptor mobility at and around the synapse (Choquet and Triller, 2003, 2013). On the nanoscale, postsynaptic AMPA receptors are thought to form dynamic clusters (Heine et al., 2008), which in many instances occur in front of the presynaptic release machinery (Tang et al., 2016). Correspondingly, it has been suggested that moderate clustering of intracleft AMPA receptors could provide an efficient mechanism to potentiate synaptic currents (Savtchenko and Rusakov, 2014).

The other key factor that determines AMPA receptor activation in the synaptic cleft is the speed with which glutamate diffuses. Until recently, this speed has been estimated from parameter optimization in models that are partially constrained by electrophysiological data and by the knowledge about extracellular diffusivity on a larger scale (Nielsen et al., 2004; Hrabetová, 2005; Kinney et al., 2013; Savtchenko et al., 2013). However, recent advances in time-resolved fluorescence anisotropy imaging have enabled measurements of quasi-instantaneous diffusivity (micro-viscosity of molecular environment) in live brain tissue (Fig. 2*A*) (Suhling et al., 2004; Zheng et al., 2014, 2017). This approach has helped to find that, in acute brain slices, small molecules on average move ~30% slower in the ECS (synaptic neuropil of hippocampal area CA1) than in a free medium (Fig. 2*B*). Because synaptic clefts represent only 1%–2% of all neuronal membranes in this area (Rusakov et al., 1998), this value reflects mainly the space outside synapses. Inside neuronal dendrites diffusion retardation increases to ~70% (Fig. 2*B*) (Zheng et al., 2017); whether this is due to the presence of cytoplasmic macromolecules or because of direct and frequent collisions with macroscopic obstacles, such as cellular organelles, remains to be

ascertained. By imaging an extracellular fluorescence probe at giant hippocampal mossy fiber synapses, these tests have found that free molecular diffusion between presynaptic and postsynaptic membranes (including the synaptic cleft and the synaptic contact areas adjacent to it) was slowed down by ~46%.

How could this estimate improve our knowledge about activation of AMPA (and other) receptors inside and outside of the synaptic cleft? Most importantly, Monte Carlo simulations replicating nanoscopic events at common central synapses (Savtchenko et al., 2013; Savtchenko and Rusakov, 2014; Zheng and Rusakov, 2015) predict a significantly broader profile of AMPA receptor activation at the experimental value of glutamate diffusivity between presynaptic and postsynaptic membranes (0.46 μm^2/ms), compared with the case of free-medium glutamate diffusivity (0.86 μm^2/ms; Fig. 2*C*). There are two main consequences of this comparison. First, it requires fewer (or a lower density of) AMPA receptors to generate the same synaptic current when the diffusion is slower than in a free medium. Second, higher medium viscosity requires much less precision for the alignment between AMPA receptors and release sites to generate a near-maximum current: incomplete exactness of such transsynaptic alignments (Tang et al., 2016) should therefore still allow for robust transmission efficacy.

La nouvelle vague: super-resolution microscopy to visualize brain ECS

The main methodologies to study brain ECS have relied either on biophysical measurements, such as real-time iontophoresis and integrative optical imaging, diffusion-weighted magnetic resonance imaging, or EM. These technologies operate on complementary scales, where the biophysical approaches can precisely quantify structural parameters, such as ECS volume fraction and tortuosity (but cannot visualize their anatomical basis), diffusion-weighted magnetic resonance imaging allows the mapping of the diffusion of water molecules in brain tissue (but only at the macro-anatomical level, and *a priori* it does not distinguish intracellular from extracellular spaces), whereas EM is capable of revealing tissue ultrastructure (but requires tissue fixation, and thus is incompatible with live dynamics).

Our current view of the nanoscale anatomy of brain ECS derives almost exclusively from EM images of chemically fixed tissue, where it appears as a uniformly thin layer (Harris and Stevens, 1989). However, EM based on cryo-fixation indicates that this is largely an artifact of the chemical fixation process, and in reality, the ECS has a heterogeneous and voluminous organization (Van Harreveld et al., 1965; Korogod et al., 2015).

By contrast, the advent of super-resolution microscopy has created unique opportunities for studying brain ECS, reconciling live-tissue imaging with nanoscale spatial resolution. Super-resolution microscopy techniques can be broadly divided into two categories, which are either based on the localization of single fluorescent emitters or on shrinking the fluorescence spot in a laser-scanning microscope. The strength of the former category (including so-called stochastic super-resolution microscopy techniques, such as (spt)PALM) (Betzig et al., 2006; Hess et al., 2006; Manley et al., 2008), (d)STORM (Rust et al., 2006; Heilemann et al., 2008), and (u/DNA)PAINT (Giannone et al., 2010; Jungmann et al., 2010), is that they not only provide positional information, but also the ability to probe the local physical and chemical environment by tracking the mobility of individual molecules over time, which makes it possible to quantify bulk properties, such as diffusivity and tortuosity. The techniques of the latter category (e.g., STED microscopy) are ideally suited for volumetric imaging of highly diffusible fluorophores, which makes it possible to visualize directly 3D cellular morphology on a rapid timescale deep inside brain slices and the intact brain *in vivo* (Nägerl et al., 2008; Tønnesen et al., 2014; Chéreau et al., 2017; Pfeiffer et al., 2018).

Super-resolution imaging of CNTs

Single-molecule tracking should in principle be suitable for revealing ECS nano-environments in live brain tissue. However, conventional probes used for single-molecule imaging do not meet the requirements, calling for new probes to be developed. We converged on single-wall CNTs as the best candidates (Godin et al., 2017). In single-molecule microscopy, one commonly uses highly luminescent probes that can be efficiently detected individually by an optical microscope. Bright organic fluorophores or QDs have been used extensively for labeling neurotransmitter receptors and revealing their dynamic behavior in neuronal cell cultures at the nanoscale (Dahan et al., 2003; Tardin et al., 2003; Groc et al., 2007; Heine et al., 2008). However, it remains challenging to perform single-molecule detection in intact brain tissue. To access the optical window of biological tissues (i.e., where tissue scattering and absorption are minimal), the use of nanoprobes with optical response in the near infrared (NIR) has become crucial, but the current red-shifted dyes are not strong emitters. The discovery of CNT fluorescence in the NIR (O'Connell et al., 2002) soon paved the way to their detection in living cells (Cherukuri et al., 2004; Duque et al., 2008). Water-solubilized CNTs display exceptionally high luminescence and photostability for a single nano-object (tens of minutes) (Cognet et al., 2007; Fakhri et al., 2010), superior to most other fluorescent nano-probes used in biological research. NIR luminescent CNTs have thus proven to be useful for ensemble imaging in whole-animal vascular systems (Welsher et al., 2009), as well as for intracellular single-molecule tracking in cultured cells (Fakhri et al., 2014). Using adequate excitation schemes in the NIR for live brain tissue imaging (Danné et al., 2018) as well as encapsulating CNTs to avoid nonspecific interactions with cellular structures, CNTs were shown to be capable of exploring the ECS nano-environment (Godin et al., 2017). CNTs are highly anisotropic with quasi one-dimensional shapes, which turned out to be a key advantage: their lengths directly impact their diffusion behaviors without compromising their access to restricted environments. It was even shown that micrometers-long CNTs can display reptation movements ("slithering like a snake") in concentrated polymer gels (Fakhri et al., 2010), as predicted by theoretical work (de Gennes, 1971). For the ECS, CNTs with lengths of 500–1000 nm were chosen because they diffuse both efficiently and at the accurate speed to be localized and tracked at video rate in the fluid environment of the ECS, which is next to impossible for spherical nanoparticles. Moreover, their hyperthin diameter (1–5 nm) confers remarkable accessibility to the "nooks and crannies" of confined ECS. These CNTs have molecular weights comparable with hyaluronan (Fraser et al., 1997), which is one of the main molecular constituents of the ECS, and have "nonsticky" surfaces that minimize nonspecific interactions with cellular microenvironments. Therefore, they are expected to act as faithful diffusion probes of the ECS at molecular scales under physiological conditions. By injecting into lateral cerebral ventricles in live animals, tissue damage and inflammation can be minimized (Varela et al., 2016). After injection, we detected CNTs in diverse areas of sagittal brain slices (e.g., the neocortex, hippocampus, striatum) far away from the original site of injection, presumably because of their tiny diameters and minimal interactions with ECS cellular

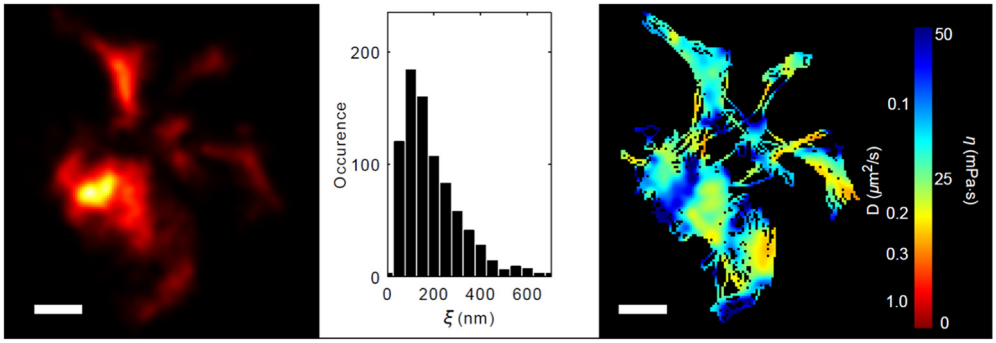

Figure 3. Super-resolution imaging of CNTs to reveal ECS structure and viscosity. ECS morphology (left) and corresponding local ECS diffusion map (right) obtained by tracking CNTs at depth (>100 μm) inside an acute brain slice from a young rat. Histogram represents the heterogeneous distribution of local ECS dimensions. Scale bars, 500 nm. Note the similarity of ECS tortuosity and sizes between Figure 3 (left panels) and Figure 1*A* (top). Reproduced with permission from Godin et al. (2017).

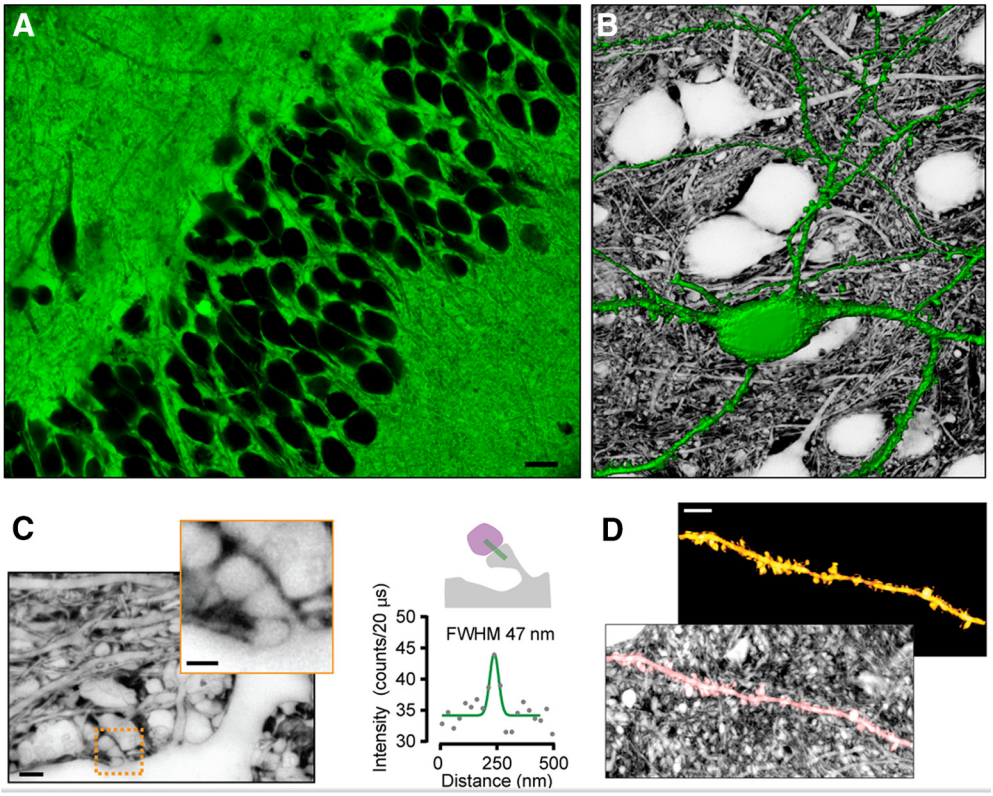

Figure 4. SUSHI of ECS and brain structures. ***A***, SUSHI is a direct way of imaging the ECS, which also visualizes brain cells "all at once." Left, Overview of the neurons of the hippocampus, which is a brain area important for memory formation. Scale bar, 10 μm. ***B***, At higher zoom and after color inversion, the image on the right reveals the micro-anatomical organization of brain tissue, including cell bodies and neuropil with nanoscale spatial resolution. The green neuron was positively labeled with a fluorescent protein and thus stands out from the rest of the inversely labeled tissue. ***C***, SUSHI enables the visualization of synaptic clefts because they are brightly labeled up against pitch-black presynaptic and postsynaptic structures (axonal boutons and dendritic spines), improving the signal-to-noise ratio for the detection of subdiffraction structures. As the look-up table was inverted to facilitate perception of contrast and structure in the images, the synaptic cleft appears dark whereas the anatomical structures are white. Scale bars: 2 μm; zoom-in, 1 μm. ***D***, SUSHI can be used to reconstruct unlabeled anatomical structures. In this example, a dendritic segment was reconstructed (top), which is overlaid with the SUSHI image of the surrounding neuropil. Scale bar, 4 μm. Reprinted with permission from Tønnesen et al. (2018).

structures. This wide spread also indicated that CNTs primarily remained in the ECS and were not taken up appreciably by brain cells. Interestingly, injecting these tracers into brain ventricles should also have promoted their localization at ECS sites distinct from perivascular regions (Iliff et al., 2012), which play a specific role in cerebrovascular physiology (Abbott et al., 2018). To report faithfully the dimensions of the ECS, we applied super-resolution localization microscopy to track CNTs in real-time during their exploration of the ECS deep (>100 μm) inside acute brain slices. We observed that ECS dimensions were not only highly heterogeneous, but also that intercell gaps were frequently >100 nm (Fig. 1), which is substantially larger than previous estimates based on QDs (Thorne and Nicholson, 2006). Super-resolved maps of the ECS obtained by CNT imaging in acute brain slices are very similar with those obtained by cryo-EM (Figs. 1*A*, 3) (Van Harreveld and Steiner, 1970; Korogod et al., 2015). In ad-

dition to revealing the nanoscale dimensions of the ECS inside acute brain slices, CNT super-resolution imaging can at the same time also provide information about the diffusive properties of the ECS (Fig. 3). Indeed, we could experimentally show that local diffusion is not only shaped by ECS dimensions but also by viscosity. In addition, CNT imaging revealed that chemical digestion of the extracellular matrix using hyaluronidase affected the diffusive properties of the ECS in a spatially inhomogeneous way (Godin et al., 2017).

In sum, our new approach makes it possible to obtain information at the same time about the nanoscale dimensions and tortuosity of the ECS in living brain tissue, revealing that the ECS is a maze of interconnected polymorphic compartments that are structured down to the nanoscale and bear specific diffusive properties.

SUSHI

To visualize directly the spatial organization of the ECS in live brain tissue, we developed SUSHI (Tønnesen et al., 2018) (Figure 4). It is based on 3D-STED microscopy, offering a volume resolution of <1 attoliter (10^{-18} liter or 0.001 μm^3), and labeling of the interstitial fluid with a diffusible fluorophore that stays outside of the cells. The labeling strategy has been used before (e.g., to measure the speed of red blood cells in brain capillaries) (Kleinfeld et al., 1998) or to visualize cell bodies for targeted patch-clamp recordings (Kitamura et al., 2008), but never in combination with super-resolution microscopy to reveal brain ECS or brain anatomy at the nanoscale.

SUSHI gives optical access to the spatial topology and dynamics of the ECS, in response to physiological stimuli, such as osmotic challenges, changes in neuronal activity, and local release of the excitatory neurotransmitter glutamate. In addition to revealing ECS structure, SUSHI also produces super-resolved images of the entire microanatomical organization of brain tissue because all cellular structures are inversely labeled and stand out like a silhouette, enabling detailed 3D reconstructions of unlabeled cells. Hence, SUSHI makes it possible to recognize various distinct extracellular compartments, including neuropil ECS and perivascular spaces.

SUSHI makes it possible to estimate the ECS volume fraction (α) in a straightforward way. In SUSHI images, α simply becomes the ratio of the number of labeled pixels to the total number of pixels for a given ROI. α ranges from 5% to 36%, with a mean of ~20% in organotypic brain slices, and shows wide regional variations across different layers of the hippocampus, consistent with previous diffusion-based studies (McBain et al., 1990; Saghyan et al., 2012; Arranz et al., 2014). It is also possible to quantify the width of the interstitial gaps separating neural structures by analyzing intensity peaks in line profiles measured across the neuropil. These gaps are highly heterogeneous, their widths ranging from ~50 nm to well >1 μm. The vast majority ($>80\%$) of them are >100 nm, which is in agreement with recent measurements in brain slices based on cryo-EM (Korogod et al., 2015) and super-resolution imaging of CNTs (Godin et al., 2017). Whether ECS widths are similar *in vivo* remains to be determined, but diffusion measurements suggest so (Nance et al., 2012).

Large reservoirs of ECS next to cell bodies can be seen in SUSHI images, which could reflect liquid-filled voids in the neuropil or contain specialized extracellular matrix structures, such as perineuronal nets. Perineuronal nets wrap around neurons and are thought to regulate neural plasticity (Dityatev et al., 2010; Sorg et al., 2016), where the pattern of holes has been proposed to be a structural correlate of long-term memories (Tsien, 2013). Interestingly, these spaces are equally visible when using fluorophores conjugated to large dextrans (with a molecular weight of 10 kDa), suggesting that they are relatively permeable structures.

SUSHI can be readily combined with other neurophysiological techniques (e.g., pharmacological experiments, electrophysiological recordings, 2-photon glutamate uncaging) to study ECS dynamics induced by physiologically meaningful stimuli. Subjecting brain tissue to an osmotic challenge (e.g., by temporarily raising the concentration of NaCl in the ACSF) is expected to draw water from cells to the ECS compartment and thus to increase ECS volume. Indeed, during hypertonic conditions, α and the interstitial spaces undergo a transient increase. In addition, elevations of neuronal activity also cause major changes in the ECS, but in the opposite direction. Brief epileptiform discharges (e.g., induced by bath-application of picrotoxin), which blocks inhibitory $GABA_A$ receptors, coincide with a marked drop in α, consistent with previous reports (Dietzel et al., 1980; Lux et al., 1986). Clustered discharges tend to induce long-lasting depression of the ECS signal (tens of minutes), whereas single discharges induce more transient changes that recover within a few minutes, even though the initial drop in ECS volume fraction is comparable. Finally, SUSHI can be used to study highly localized activity-driven changes in ECS structure, induced by 2-photon glutamate uncaging, which mimics the release of glutamate from single synaptic terminals.

So far, we have applied SUSHI only to brain slices, but it should also work in the intact brain by adapting cranial window approaches and 3D-STED microscopy *in vivo* (Pfeiffer et al., 2018), the main limitations being imaging depth and brain motion. The use of adaptive optics (Gould et al., 2012; Patton et al., 2016) and 2-photon STED microscopy (Bethge et al., 2013; Takasaki et al., 2013) as well as optimized surgery and labeling techniques are bound to help overcome these hurdles.

In conclusion, it is clear that studying the ECS holds great promise for fundamental neuroscience as well as translational research aimed at identifying new drug targets and diagnostic read-outs for brain diseases. In as much as the ECS becomes more experimentally tractable with the development of new biosensors, imaging technology, and modeling approaches, it will increasingly attract the attention from neuroscientists and funding agencies, leading to essential new insights into how the brain works. The prospects for that have never been better.

References

Abbott NJ, Pizzo ME, Preston JE, Janigro D, Thorne RG (2018) The role of brain barriers in fluid movement in the CNS: is there a 'glymphatic' system? Acta Neuropathol 135:387–407. CrossRef Medline

Arranz AM, Perkins KL, Irie F, Lewis DP, Hrabe J, Xiao F, Itano N, Kimata K, Hrabetová S, Yamaguchi Y (2014) Hyaluronan deficiency due to Has3 knock-out causes altered neuronal activity and seizures via reduction in brain extracellular space. J Neurosci 34:6164–6176. CrossRef Medline

Bethge P, Chéreau R, Avignone E, Marsicano G, Nägerl UV (2013) Two-photon excitation STED microscopy in two colors in acute brain slices. Biophys J 104:778–785. CrossRef Medline

Betzig E, Patterson GH, Sougrat R, Lindwasser OW, Olenych S, Bonifacino JS, Davidson MW, Lippincott-Schwartz J, Hess HF (2006) Imaging intracellular fluorescent proteins at nanometer resolution. Science 313:1642–1645. CrossRef Medline

Chéreau R, Saraceno GE, Angibaud J, Cattaert D, Nägerl UV (2017) Super-resolution imaging reveals activity-dependent plasticity of axon morphology linked to changes in action potential conduction velocity. Proc Natl Acad Sci U S A 114:1401–1406. CrossRef Medline

Cherukuri P, Bachilo SM, Litovsky SH, Weisman RB (2004) Near-infrared fluorescence microscopy of single-walled carbon nanotubes in phagocytic cells. J Am Chem Soc 126:15638–15639. CrossRef Medline

Choquet D, Triller A (2003) The role of receptor diffusion in the organiza-

tion of the postsynaptic membrane. Nat Rev Neurosci 4:251–265. CrossRef Medline

Choquet D, Triller A (2013) The dynamic synapse. Neuron 80:691–703. CrossRef Medline

Clements JD (1996) Transmitter timecourse in the synaptic cleft: its role in central synaptic function. Trends Neurosci 5:163–170. CrossRef Medline

Cognet L, Tsyboulski DA, Rocha JD, Doyle CD, Tour JM, Weisman RB (2007) Stepwise quenching of exciton fluorescence in carbon nanotubes by single-molecule reactions. Science 316:1465–1468. CrossRef Medline

Dahan M, Lévi S, Luccardini C, Rostaing P, Riveau B, Triller A (2003) Diffusion dynamics of glycine receptors revealed by single-quantum dot tracking. Science 302:442–445. CrossRef Medline

Danné N, Godin AG, Gao Z, Varela JA, Groc L, Lounis B, Cognet L (2018) Comparative analysis of photoluminescence and up-conversion emission from individual carbon nanotubes for bio-imaging applications. ACS Photonics 5:359–364. CrossRef

de Gennes PG (1971) Reptation of a polymer chain in the presence of fixed obstacles. J Chem Phys 55:572.

de Gennes PG (1979) Scaling concepts in polymer physics. Ithaca, NY: Cornell UP.

Dechadilok P, Deen WM (2006) Hindrance factors for diffusion and convection in pores. Ind Eng Chem Res 45:6953–6959. CrossRef

Deen WM (1987) Hindered transport of large molecules in liquid filled pores. AIChE J 33:1409–1425. CrossRef

Dietzel I, Heinemann U, Hofmeier G, Lux HD (1980) Transient changes in the size of the extracellular space in the sensorimotor cortex of cats in relation to stimulus-induced changes in potassium concentration. Exp Brain Res 40:432–439. Medline

Dityatev A, Schachner M, Sonderegger P (2010) The dual role of the extracellular matrix in synaptic plasticity and homeostasis. Nat Rev Neurosci 11:735–746. CrossRef Medline

Duque JG, Cognet L, Parra-Vasquez AN, Nicholas N, Schmidt HK, Pasquali M (2008) Stable luminescence from individual carbon nanotubes in acidic, basic, and biological environments. J Am Chem Soc 130:2626–2633. CrossRef Medline

Fakhri N, MacKintosh FC, Lounis B, Cognet L, Pasquali M (2010) Brownian motion of stiff filaments in a crowded environment. Science 330:1804–1807. CrossRef Medline

Fakhri N, Wessel AD, Willms C, Pasquali M, Klopfenstein DR, MacKintosh FC, Schmidt CF (2014) High-resolution mapping of intracellular fluctuations using carbon nanotubes. Science 344:1031–1035. CrossRef Medline

Ferrer-Ferrer M, Dityatev A (2018) Shaping synapses by the neural extracellular matrix. Front Neuroanat 12:40. CrossRef Medline

Fraser JR, Laurent TC, Laurent UB (1997) Hyaluronan: its nature, distribution, functions and turnover. J Intern Med 242:27–33. CrossRef Medline

Giannone G, Hosy E, Levet F, Constals A, Schulze K, Sobolevsky AI, Rosconi MP, Gouaux E, Tampé R, Choquet D, Cognet L (2010) Dynamic superresolution imaging of endogenous proteins on living cells at ultra-high density. Biophys J 99:1303–1310. CrossRef Medline

Godin AG, Varela JA, Gao Z, Danné N, Dupuis JP, Lounis B, Groc L, Cognet L (2017) Single-nanotube tracking reveals the nanoscale organization of the extracellular space in the live brain. Nat Nanotechnol 12:238–243. CrossRef Medline

Gould TJ, Burke D, Bewersdorf J, Booth MJ (2012) Adaptive optics enables 3D STED microscopy in aberrating specimens. Opt Express 20:20998–21009. CrossRef Medline

Groc L, Lafourcade M, Heine M, Renner M, Racine V, Sibarita JB, Lounis B, Choquet D, Cognet L (2007) Surface trafficking of neurotransmitter receptor: comparison between single-molecule/quantum dot strategies. J Neurosci 27:12433–12437. CrossRef Medline

Harris KM, Stevens JK (1989) Dendritic spines of CA 1 pyramidal cells in the rat hippocampus: serial electron microscopy with reference to their biophysical characteristics. J Neurosci 9:2982–2997. CrossRef Medline

Heilemann M, van de Linde S, Schüttpelz M, Kasper R, Seefeldt B, Mukherjee A, Tinnefeld P, Sauer M (2008) Subdiffraction-resolution fluorescence imaging with conventional fluorescent probes. Angew Chem Int Ed Engl 47:6172–6176. CrossRef Medline

Heine M, Groc L, Frischknecht R, Béïque JC, Lounis B, Rumbaugh G, Huganir RL, Cognet L, Choquet D (2008) Surface mobility of postsynaptic AMPARs tunes synaptic transmission. Science 320:201–205. CrossRef Medline

Hess ST, Girirajan TP, Mason MD (2006) Ultra-high resolution imaging by fluorescence photoactivation localization microscopy. Biophys J 91:4258–4272. CrossRef Medline

Hrabe J, Hrabetová S, Segeth K (2004) A model of effective diffusion and tortuosity in the extracellular space of the brain. Biophys J 87:1606–1617. CrossRef Medline

Hrabetová S (2005) Extracellular diffusion is fast and isotropic in the stratum radiatum of hippocampal CA1 region in rat brain slices. Hippocampus 15:441–450. CrossRef Medline

Hrabetová S, Nicholson C (2004) Contribution of dead-space microdomains to tortuosity of brain extracellular space. Neurochem Int 45:467–477. CrossRef Medline

Hrabetová S, Hrabe J, Nicholson C (2003) Dead-space microdomains hinder extracellular diffusion in rat neocortex during ischemia. J Neurosci 23:8351–8359. CrossRef Medline

Hrabetová S, Masri D, Tao L, Xiao F, Nicholson C (2009) Calcium diffusion enhanced after cleavage of negatively charged components of brain extracellular matrix by chondroitinase ABC. J Physiol 587:4029–4049. CrossRef Medline

Iliff JJ, Wang M, Liao Y, Plogg BA, Peng W, Gundersen GA, Benveniste H, Vates GE, Deane R, Goldman SA, Nagelhus EA, Nedergaard M (2012) A paravascular pathway facilitates CSF flow through the brain parenchyma and the clearance of interstitial solutes, including amyloid beta. Sci Transl Med 4:147ra111. CrossRef Medline

Iliff JJ, Chen MJ, Plog BA, Zeppenfeld DM, Soltero M, Yang L, Singh I, Deane R, Nedergaard M (2014) Impairment of glymphatic pathway function promotes tau pathology after traumatic brain injury. J Neurosci 34:16180–16193. CrossRef Medline

Jefferys JG (1995) Nonsynaptic modulation of neuronal activity in the brain: electric currents and extracellular ions. Physiol Rev 75:689–723. CrossRef Medline

Jungmann R, Steinhauer C, Scheible M, Kuzyk A, Tinnefeld P, Simmel FC (2010) Single-molecule kinetics and super-resolution microscopy by fluorescence imaging of transient binding on DNA origami. Nano Lett 10:4756–4761. CrossRef Medline

Kinney JP, Spacek J, Bartol TM, Bajaj CL, Harris KM, Sejnowski TJ (2013) Extracellular sheets and tunnels modulate glutamate diffusion in hippocampal neuropil. J Comp Neurol 521:448–464. CrossRef Medline

Kitamura K, Judkewitz B, Kano M, Denk W, Häusser M (2008) Targeted patch-clamp recordings and single-cell electroporation of unlabeled neurons in vivo. Nat Methods 5:61–67. CrossRef Medline

Kleinfeld D, Mitra PP, Helmchen F, Denk W (1998) Fluctuations and stimulus-induced changes in blood flow observed in individual capillaries in layers 2 through 4 of rat neocortex. Proc Natl Acad Sci U S A 95:15741–15746. CrossRef Medline

Korogod N, Petersen CC, Knott GW (2015) Ultrastructural analysis of adult mouse neocortex comparing aldehyde perfusion with cryo fixation. eLife 4.

Lux HD, Heinemann U, Dietzel I (1986) Ionic changes and alterations in the size of the extracellular space during epileptic activity. Adv Neurol 44:619–639. Medline

Manley S, Gillette JM, Patterson GH, Shroff H, Hess HF, Betzig E, Lippincott-Schwartz J (2008) High-density mapping of single-molecule trajectories with photoactivated localization microscopy. Nat Methods 5:155–157. CrossRef Medline

McBain CJ, Traynelis SF, Dingledine R (1990) Regional variation of extracellular space in the hippocampus. Science 249:674–677. CrossRef Medline

Nägerl UV, Willig KI, Hein B, Hell SW, Bonhoeffer T (2008) Live-cell imaging of dendritic spines by STED microscopy. Proc Natl Acad Sci U S A 105:18982–18987. CrossRef Medline

Nance EA, Woodworth GF, Sailor KA, Shih TY, Xu Q, Swaminathan G, Xiang D, Eberhart C, Hanes J (2012) A dense poly(ethylene glycol) coating improves penetration of large polymeric nanoparticles within brain tissue. Sci Transl Med 4:149ra119. CrossRef Medline

Nicholson C, Hrabetová S (2017) Brain extracellular space: the final frontier of neuroscience. Biophys J 113:2133–2142. CrossRef Medline

Nicholson C, Phillips JM (1981) Ion diffusion modified by tortuosity and volume fraction in the extracellular microenvironment of the rat cerebellum. J Physiol 321:225–257. CrossRef Medline

Nicholson C, Tao L (1993) Hindered diffusion of high molecular weight compounds in brain extracellular microenvironment measured with integrative optical imaging. Biophys J 65:2277–2290. CrossRef Medline

Nielsen TA, DiGregorio DA, Silver RA (2004) Modulation of glutamate mobility reveals the mechanism underlying slow-rising AMPAR EPSCs and the diffusion coefficient in the synaptic cleft. Neuron 42:757–771. CrossRef Medline

O'Connell MJ, Bachilo SM, Huffman CB, Moore VC, Strano MS, Haroz EH, Rialon KL, Boul PJ, Noon WH, Kittrell C, Ma J, Hauge RH, Weisman RB, Smalley RE (2002) Band gap fluorescence from individual single-walled carbon nanotubes. Science 297:593–596. CrossRef Medline

Odackal J, Colbourn R, Odackal NJ, Tao L, Nicholson C, Hrabetová S (2017) Real-time iontophoresis with tetramethylammonium to quantify volume fraction and tortuosity of brain extracellular space. J Vis Exp 125.

Patton BR, Burke D, Owald D, Gould TJ, Bewersdorf J, Booth MJ (2016) Three-dimensional STED microscopy of aberrating tissue using dual adaptive optics. Opt Express 24:8862–8876. CrossRef Medline

Perkins KL, Arranz AM, Yamaguchi Y, Hrabetová S (2017) Brain extracellular space, hyaluronan, and the prevention of epileptic seizures. Rev Neurosci 28:869–892. CrossRef Medline

Pfeiffer T, Poll S, Bancelin S, Angibaud J, Inavalli VK, Keppler K, Mittag M, Fuhrmann M, Nägerl UV (2018) Chronic 2P-STED imaging reveals high turnover of dendritic spines in the hippocampus in vivo. eLife 7:e34700. CrossRef Medline

Raghavachari S, Lisman JE (2004) Properties of quantal transmission at CA1 synapses. J Neurophysiol 92:2456–2467. CrossRef Medline

Rusakov DA (2001) The role of perisynaptic glial sheaths in glutamate spillover and extracellular Ca^{2+} depletion. Biophys J 81:1947–1959. CrossRef Medline

Rusakov DA, Kullmann DM (1998) Geometric and viscous components of the tortuosity of the extracellular space in the brain. Proc Natl Acad Sci U S A 95:8975–8980. CrossRef Medline

Rusakov DA, Harrison E, Stewart MG (1998) Synapses in hippocampus occupy only 1–2% of cell membranes and are spaced less than half-micron apart: a quantitative ultrastructural analysis with discussion of physiological implications. Neuropharmacology 37:513–521. CrossRef Medline

Rust MJ, Bates M, Zhuang X (2006) Sub-diffraction-limit imaging by stochastic optical reconstruction microscopy (STORM). Nat Methods 3:793–795. CrossRef Medline

Saghyan A, Lewis DP, Hrabe J, Hrabetová S (2012) Extracellular diffusion in laminar brain structures exemplified by hippocampus. J Neurosci Methods 205:110–118. CrossRef Medline

Savtchenko LP, Rusakov DA (2014) Moderate AMPA receptor clustering on the nanoscale can efficiently potentiate synaptic current. Philos Trans R Soc Lond B Biol Sci 369:20130167. CrossRef Medline

Savtchenko LP, Sylantyev S, Rusakov DA (2013) Central synapses release a resource-efficient amount of glutamate. Nat Neurosci 16:10–12. CrossRef Medline

Sorg BA, Berretta S, Blacktop JM, Fawcett JW, Kitagawa H, Kwok JC, Miquel M (2016) Casting a wide net: role of perineuronal nets in neural plasticity. J Neurosci 36:11459–11468. CrossRef Medline

Stiles JR, Bartol TM (2001) Monte Carlo methods for simulating realistic synaptic microphysiology using MCell. In: Computational neuroscience: realistic modeling for experimentalists computational neuroscience (De Schutter, E, ed), pp 87–127. Realistic modeling for experimentalists. Boca Raton, FL: CRC.

Suhling K, Siegel J, Lanigan PM, Lévêque-Fort S, Webb SE, Phillips D, Davis DM, French PM (2004) Time-resolved fluorescence anisotropy imaging applied to live cells. Opt Lett 29:584–586. CrossRef Medline

Suhling K, Hirvonen LM, Levitt JA, Chung PH, Tregidgo C, Le Marois A, Rusakov DA, Zheng K, Ameer-Beg S, Poland S (2015) Fluorescence lifetime imaging (FLIM): Basic concepts and some recent developments. Med Photonics 27:3–40.

Syková E, Nicholson C (2008) Diffusion in brain extracellular space. Physiol Rev 88:1277–1340. CrossRef Medline

Takasaki KT, Ding JB, Sabatini BL (2013) Live-cell superresolution imaging by pulsed STED two-photon excitation microscopy. Biophys J 104:770–777. CrossRef Medline

Tang AH, Chen H, Li TP, Metzbower SR, MacGillavry HD, Blanpied TA (2016) A trans-synaptic nanocolumn aligns neurotransmitter release to receptors. Nature 536:210–214. CrossRef Medline

Tao A, Tao L, Nicholson C (2005) Cell cavities increase tortuosity in brain extracellular space. J Theor Biol 234:525–536. CrossRef Medline

Tao L, Nicholson C (2004) Maximum geometrical hindrance to diffusion in brain extracellular space surrounding uniformly spaced convex cells. J Theor Biol 229:59–68. CrossRef Medline

Tardin C, Cognet L, Bats C, Lounis B, Choquet D (2003) Direct imaging of lateral movements of AMPA receptors inside synapses. EMBO J 22:4656–4665. CrossRef Medline

Thorne RG, Nicholson C (2006) In vivo diffusion analysis with quantum dots and dextrans predicts the width of brain extracellular space. Proc Natl Acad Sci U S A 103:5567–5572. CrossRef Medline

Thorne RG, Lakkaraju A, Rodriguez-Boulan E, Nicholson C (2008) In vivo diffusion of lactoferrin in brain extracellular space is regulated by interactions with heparan sulfate. Proc Natl Acad Sci U S A 105:8416–8421. CrossRef Medline

Tønnesen J, Katona G, Rózsa B, Nägerl UV (2014) Spine neck plasticity regulates compartmentalization of synapses. Nat Neurosci 17:678–685. CrossRef Medline

Tønnesen J, Inavalli VV, Nägerl UV (2018) Super-resolution imaging of the extracellular space in living brain tissue. Cell 172:1108–1121.e15. CrossRef Medline

Toole BP (2004) Hyaluronan: from extracellular glue to pericellular cue. Nat Rev Cancer 4:528–539. CrossRef Medline

Trommershäuser J, Marienhagen J, Zippelius A (1999) Stochastic model of central synapses: slow diffusion of transmitter interacting with spatially distributed receptors and transporters. J Theor Biol 198:101–120. CrossRef Medline

Tsien RY (2013) Very long-term memories may be stored in the pattern of holes in the perineuronal net. Proc Natl Acad Sci U S A 110:12456–12461. CrossRef Medline

Van Harreveld A, Steiner J (1970) The magnitude of the extracellular space in electron micrographs of superficial and deep regions of the cerebral cortex. J Cell Sci 6:793–805. Medline

Van Harreveld A, Crowell J, Malhotra SK (1965) A study of extracellular space in central nervous tissue by freeze-substitution. J Cell Biol 25:117–137. CrossRef Medline

Varela JA, Dupuis JP, Etchepare L, Espana A, Cognet L, Groc L (2016) Targeting neurotransmitter receptors with nanoparticles in vivo allows single-molecule tracking in acute brain slices. Nat Commun 7:10947. CrossRef Medline

Vedunova M, Sakharnova T, Mitroshina E, Perminova M, Pimashkin A, Zakharov Y, Dityatev A, Mukhina I (2013) Seizure-like activity in hyaluronidase-treated dissociated hippocampal cultures. Front Cell Neurosci 7:149. CrossRef Medline

Wahl LM, Pouzat C, Stratford KJ (1996) Monte Carlo simulation of fast excitatory synaptic transmission at a hippocampal synapse. J Neurophysiol 75:597–608. CrossRef Medline

Welsher K, Liu Z, Sherlock SP, Robinson JT, Chen Z, Daranciang D, Dai H (2009) A route to brightly fluorescent carbon nanotubes for near-infrared imaging in mice. Nat Nanotechnol 4:773–780. CrossRef Medline

Xiao F, Nicholson C, Hrabe J, Hrabetová S (2008) Diffusion of flexible random-coil dextran polymers measured in anisotropic brain extracellular space by integrative optical imaging. Biophys J 95:1382–1392. CrossRef Medline

Xiao F, Hrabe J, Hrabetová S (2015) Anomalous extracellular diffusion in rat cerebellum. Biophys J 108:2384–2395. CrossRef Medline

Xie L, Kang H, Xu Q, Chen MJ, Liao Y, Thiyagarajan M, O'Donnell J, Christensen DJ, Nicholson C, Iliff JJ, Takano T, Deane R, Nedergaard M (2013) Sleep drives metabolite clearance from the adult brain. Science 342:373–377. CrossRef Medline

Zheng K, Rusakov DA (2015) Efficient integration of synaptic events by NMDA receptors in three-dimensional neuropil. Biophys J 108:2457–2464. CrossRef Medline

Zheng K, Scimemi A, Rusakov DA (2008) Receptor actions of synaptically released glutamate: the role of transporters on the scale from nanometers to microns. Biophys J 95:4584–4596. CrossRef Medline

Zheng K, Levitt JA, Suhling K, Rusakov DA (2014) Monitoring nanoscale mobility of small molecules in organized brain tissue with time-resolved fluorescence anisotropy imaging. In: Nanoscale imaging of synapses, pp 125–143. New York: Springer.

Zheng K, Jensen TP, Savtchenko LP, Levitt JA, Suhling K, Rusakov DA (2017) Nanoscale diffusion in the synaptic cleft and beyond measured with time-resolved fluorescence anisotropy imaging. Sci Rep 7:42022. CrossRef Medline